Eur. Phys. J. B **14**, 483–493 (2000)

THE EUROPEAN PHYSICAL JOURNAL B

EDP Sciences

Physical properties of skutteruditesYb$_x$M$_4$Sb$_{12}$, M = Fe, Co, Rh, Ir

E. Bauer[1,a], A. Galatanu[1,b], H. Michor[1], G. Hilscher[1], P. Rogl[2], P. Boulet[2,c], and H. Noël[3]

[1] Institut für Experimentalphysik, Technische Universität Wien, 1040 Wien, Austria
[2] Institut für Physikalische Chemie, Universität Wien, Währingerstraße 42, 1090 Wien, Austria
[3] Laboratoire de Chimie du Solide et Inorganique Moléculaire[d], Université de Rennes 1, avenue du Général Leclerc, 35042 Rennes, France

Received 15 July 1999

Abstract. A series of compounds $Yb_xM_4Sb_{12}$, M = Fe, Co, FeCo, Rh, Ir, were synthesised by reaction sintering. From Rietveld refinements isotypism was determined in all cases with the $LaFe_4P_{12}$-(skutterudite)-type, space group $Im\bar{3}$ – No. 204. These refinements also served to derive the Yb-content in the samples. There is a systematic trend for the Yb-occupancy in the parent lattice M_4Sb_{12}, revealing a gradual decrease of the Yb-content from $x = 0.8$ (M = Fe), $x = 0.5$ (FeCo), $x = 0.2$ (Co), $x = 0.1$ (Rh) to $x \approx 0.02$ (Ir). This dependency seems to correlate with the thermal stability of the ternary compounds: a true ternary compound forms for M = Fe, whilst for M = Co, Rh, Ir stable binary skutterudite compounds MSb_3 already exist. Measurements of various bulk properties revealed the absence of any long range magnetic order in this series of compounds. While the samples rich in Yb behave metallic like, the Rh and Ir based skutterudites show a semiconducting-like resistivity which at lower temperatures is characterised by variable range hopping in the presence of strong Coulomb interaction. Although $Yb_{0.1}Rh_4Sb_{12}$ exhibits a Seebeck coefficient up to about 150 μV/K, figures of merit ZT generally are below 0.1 near room temperature, primarily due to the large resistivities of the sintered material.

PACS. 72.15.Eb Electrical and thermal conduction in crystalline metals and alloys – 72.15.Jf Thermoelectric and thermomagnetic effects – 84.60.Bk Performance characteristics of energy conversion systems; figure of merit

1 Introduction

Ternary metal pnictides with the general formula REM_4X_{12} (RE = rare earth, M = transition metals and X = pnicogen) crystallise in the cubic skutterudite structure, filled by rare earth atoms. Various exciting physical properties were found for this class of compounds, among them are superconductivity [1–3], metal-insulator transition [4] or heavy fermion behaviour [5–8]. Some of these compounds are found to exhibit substantially enhanced values of the figure of merit $Z = S^2/\rho\lambda$, ranking these materials among potential candidates for thermoelectric applications (S: coefficient of the thermopower, ρ: coefficient of the electrical resistivity and λ: coefficient of the thermal conductivity). For a recent review see *e.g.* Sales *et al.* [9]. Beside their large thermopower values, these compounds are characterised by a reduced thermal conductivity of the lattice due to the fact that the rare earth metals exhibit exceptionally large thermal parameters, corresponding to a "rattling" (*i.e.*, soft phonon mode) of these atoms in an oversized cage [10].

In previous investigations it has been shown that the skutterudite structure is stable as long as the large (light) rare earth atoms are involved. Due to the lanthanide contraction, the volume of the heavier rare earth ions is reduced and as a consequence, their smaller radii prevent adequate bonding to the lattice [8]. However, Tm and Yb frequently behave divalently and their respective volume may be comparable to the light rare earth ions. In fact, Dilley *et al.* [8] and Leithe-Jasper *et al.* [11] have shown that $YbFe_4Sb_{12}$ crystallises in the cubic skutterudite structure with space group $Im\bar{3}$ and the valence of the Yb ion is supposed to be intermediate between di- and trivalent. From a single crystal study [11] a complete site occupation was deduced for Yb in $YbFe_4Sb_{12}$, whereas, as already pointed out previously [12–15], the filling of rare earth ions in the cages of the skutterudite structure formed by M-X octahedra may generally not be complete. Since the rare earth ions are expected to provide electrons

[a] e-mail: bauer@xphys.tuwien.ac.at
[b] *Permanent address*: National Institute for Materials Physics, 76900 Bucarest-Magurele, Romania
[c] *Permanent address*: Laboratoire de Chimie du Solide et Inorganique Moléculaire, UMR CNRS 1495, Université de Rennes, 35042 Rennes, France
[d] UMR CNRS 1495

for the band (3 in a normal rare earth metal), electronic and magnetic properties may depend sensitively on the particular rare earth content. With respect to technical applications changes of the electron or hole count may be used for an optimisation of the figure of merit.

In this paper we show that new Yb-based skutterudites exist for M = Co, Rh and Ir, and a solid solution is possible for $Yb(Fe,Co)_4Sb_{12}$. Transport and thermodynamic properties of these compounds are studied and the magnetic state of the Yb ion and the polyanion $[M_4Sb_{12}]$ is discussed. Moreover, we evaluate the figure of merit Z for some compounds of this series which determines their technical applicability.

2 Experimental

2.1 Synthesis

Starting materials were fine filings from Yb-ingots, supplied by Auer-Remy, D, (99.9 wt%) and metal-powders (99.9 wt%, Fe, Co, Rh, Ir and Sb) purchased from Johnson & Matthey, UK. Due to the high vapour pressure of Yb and Sb at elevated temperatures, production by the conventional arc furnace method was ruled out. Therefore the material was synthesised by reaction sintering of intimate mixtures of the stoichiometric amounts of the filings and powders, which were compacted to pellets without the use of any lubricant in a steel die. The tablets, each of a weight of 1–2 g, were then sealed under vacuum in silica capsules. The samples were slowly heated to 600 °C at 50 °C/h and kept there for 150 hours. After this initial heating the cooled products were repowdered and repressed into pellets which were then annealed in evacuated quartz ampoules at 650 °C for 150 hours followed by quenching in water. The pellets were found to be in a dense sintered state. The samples were generally inspected by light optical microscopy and X-ray diffraction. Only minor amounts of impurity phases such as $YbSb_2$, FeSb or $FeSb_2$ or Yb_2O_3 were identified by EMPA (electron microprobe analysis), which hardly showed in the X-ray powder diagrams. It is noteworthy that the overall amount of Yb in the skutterudite phase is only 5.88 atom % (for full occupation of the 2a sites). Even small amounts of secondary phases, formed in the preparation, thus may consume a significant part of the Yb and thus may substantially contribute to the magnetic properties of the bulk material (see below).

2.2 X-ray powder diffraction

X-ray powder diffraction data were obtained using a Huber Guinier powder camera applying monochromatic CuK_{α_1} radiation with an image plate recording system. Lattice parameters were calculated by least squares fits to the indexed 4Θ-values applying the program package STRUKTUR [16]. For quantitative refinement of the atom positions, X-ray intensities were recorded from a flat specimen in a Siemens D5000 automatic powder diffractometer (CuK_α) or taken from the Guinier image plate recordings. For a refinement of the X-ray data we employed the FULLPROF program [17] on the base of our single crystal data of $YbFe_4Sb_{12}$ [11].

2.3 Measurement of bulk properties

The electrical resistivity and magnetoresistivity of bar shaped samples were measured using a four probe d.c. method in the temperature range from 1 K to room temperature and fields up to 12 T.

The thermal conductivity measurements were performed in a flow cryostat on cuboid-shaped samples (length: about 1 cm, cross-section: about 2 mm^2), which where kept cold by anchoring one end of the sample onto a thick copper panel mounted on the heat exchanger of the cryostat. The temperature difference along the sample, established by electrical heating, was determined by means of a differential thermocouple (Au + 0.07 %Fe/Chromel).

Thermopower measurements were carried out in a differential method. The absolute thermopower $S_x(T)$ was calculated using the following equation: $S_x(T) = S_{\mathrm{Pb}}(T) - V_{\mathrm{Pb}/x}/\Delta T$ where S_{Pb} is the absolute thermopower of lead and $V_{\mathrm{Pb}/x}$ is the thermally induced voltage across the sample, depending on the temperature difference ΔT.

A SQUID magnetometer served for the determination of the magnetisation from 2 K up to 300 K in fields up to 6 T. Specific heat measurements on samples of about 1–2 g were performed at temperatures ranging from 1.5 K up to 60 K by means of a quasi-adiabatic step-heating technique.

3 Results and discussion

3.1 Structural chemistry

The obtained X-ray intensity pattern could be easily indexed on the basis of a body-centred cubic lattice prompting isotypism with $LaFe_4P_{12}$ [18]. The refinements of the X-ray intensities in all cases converged satisfactorily for a fully ordered atom arrangement with respect to atom site distribution among Yb, M and Sb atoms (Tab. 1). Occupation factors were refined and for all compounds studied correspond to a full occupancy of the M and Sb sublattice but reveal considerable voids for the Yb-sites. Due to the usually strong correlation with temperature factors B_{ij}, the occupancies were kept fixed in the final runs to refine the B_{ij} values. The crystal structure of $YbFe_4Sb_{12}$ is shown in Figure 1 and the interatomic distances are listed in Table 1. The structure is composed of a three-dimensional array of distorted $FeSb_6$ corner-sharing octahedra which are tilted. This structural peculiarity gives rise to the formation of a rectangular arrangement of planar Sb_4 units which connect adjacent octahedra. The large electropositive rare earth cation is located in the nearly icosahedral voids formed by this atomic arrangement. A detailed discussion of the crystallo-chemical relations between the ternary filled skutterudites and the $CaTiO_3$

Table 1. Structural data (Rietveld refinements) for Yb$_x$M$_4$Sb$_{12}$compounds; (M = Fe, Co, Rh, Ir; $CoAs_3$ – type, space group: I m $\bar{3}$); data collection from Guinier image plate with CuK$_{\alpha_1}$; range of scattering angle $8 \leq 2\Theta \leq 100$.

Parameter/compound	$Yb_{0.8}Fe_4Sb_{12}$	$Yb_{0.5}Fe_2Co_2Sb_{12}$	$Yb_{0.2}Co_4Sb_{12}$	$Yb_{0.1}Rh_4Sb_{12}$	$Yb_{0.02}Ir_4Sb_{12}$
Lattice parameter a [nm]	0.914971(6)	0.90858(1)	0.904878(1)	0.922890(6)	0.924319(5)
Unit cell volume V [nm^3]	0.76599(1)	0.75005(2)	0.74092(1)	0.786049(8)	0.789706(8)
X-ray density ρ_x [Mgm^{-3}]	7.92	7.85	7.76	7.98	9.38
Reflections measured	84	81	81	86	86
Number of variables in refinement	28	29	30	23	21
Residual values R_i (Rietveld refinement)					
$R_F = \sum \lvert F_0 - F_c \rvert / \sum F_0$	0.031	0.073	0.088	0.043	0.044
$R_I = \sum \lvert I_{0B} - I_{cB} \rvert / \sum I_{0B}$	0.038	0.091	0.106	0.058	0.074
$R_{wP} = \left[\sum w_i \lvert Y_{oi} - Y_{ci} \rvert^2 / \sum w_i \lvert Y_{oi} \rvert^2\right]^{1/2}$	0.187	0.177	0.207	0.239	0.152
$R_P = \sum \lvert Y_{0i} - Y_{ci} \rvert / \sum \lvert Y_{0i} \rvert$	0.182	0.194	0.265	0.220	0.136
$R_e = \left[(N - P + C) / \sum w_i Y_{0i}^2)\right]^{1/2}$	0.045	0.048	0.051	0.045	0.030
Goodness of fit $\chi^2 = (R_{wP}/R_e)^2$	17.4	13.7	16.4	28.9	25.4
Atom parameters					
Yb in site 2a (0,0,0)	–	–	–	–	
Isotropic thermal coefficient $B_{\rm iso}$	1.50(7)	2.23(8)	0.43(6)	0.47(5)	0.43(3)
occupancy	0.827(3)	0.481(2)	0.193(4)	0.09(4)	0.02(2)
M in site 8c (1/4, 1/4, 1/4)	Fe	4Fe + 4Co	Co	Rh	Ir
$B_{\rm iso}$	1.27(6)	0.73(3)	0.36(4)	1.21(3)	0.23 (3)
occupancy	1.0	1.0	1.0	1.0	1.0
Sb in site 24 g (0,y,z) y:	0.1591(1)	0.15743(5)	0.15729(9)	0.15390(9)	0.15306(7)
z:	0.3354(1)	0.33605(6)	0.33509(9)	0.33925(9)	0.33974(8)
$B_{\rm iso}$	1.71(2)	0.21(2)	0.42(2)	1.33(2)	0.33(2)
occupancy	1.0	1.0	1.0	1.0	1.0
Interatomic distances [nm]; standard deviations generally < 0.0005 nm					
Yb - 12 Sb	0.3396	0.3372	0.3350	0.3438	0.3444
Yb - 8 M	0.3962	0.3934	0.3918	0.3996	0.4002
M - 6 Sb	0.2556	0.2545	0.2533	0.2605	0.2614
M - 2 Yb	0.3962	0.3934	0.3918	0.3996	0.4002
Sb - 2 M	0.2556	0.2545	0.2533	0.2605	0.2614
Sb - 1 Sb	0.2911	0.2861	0.2846	0.2841	0.2830
Sb - 1 Sb	0.3013	0.2979	0.2984	0.2961	0.2963
Sb - 1 Yb	0.3396	0.3372	0.3350	0.3438	0.3444

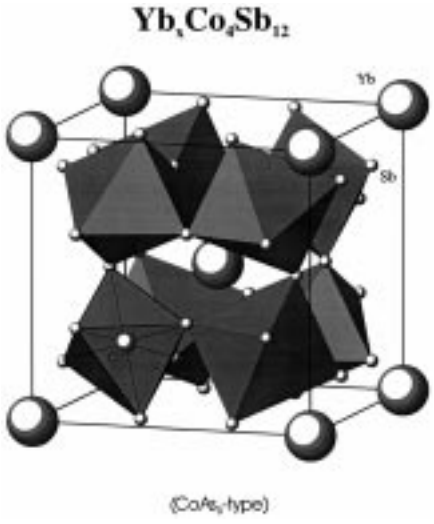

Fig. 1. Crystal structure of $YbFe_4Sb_{12}$ in a three dimensional view. The octahedral coordination around the Fe ions is outlined.

perovskites is given in [18]. As typical for the family of filled skutterudites the large electropositive cation $[Yb]^{x+}$ has to be accommodated in the $[M_4Sb_{12}]^{x-}$ polyanionic framework where the Yb atom is co-ordinated by 12 Sb atoms. From a recent analysis [11] of the interatomic distances in $YbFe_4Sb_{12}$, with full Yb stoichiometry, the Yb-Sb distance 0.3409 nm was found to be significantly larger than in binary $YbSb_2$, giving rise to rather high thermal parameters for the Yb atom in $YbFe_4Sb_{12}$. For all filled skutterudites a similar situation is observed, where the Yb atoms seem to rattle in oversized voids formed by the Sb sublattice. Whereas in a subtle preparation at rather low temperatures *via* precursor compounds a full occupancy was obtained for $YbFe_4Sb_{12}$ [11], the production route at higher temperatures adopted throughout this paper resulted in only an eighty percent filling of the Yb-site in our iron containing compound. For constant preparation procedures a systematic decrease in Yb occupancy was noted for the sequence Fe, FeCo, Co, Rh, Ir, becoming almost zero for the Ir-compound (see Tab. 1). This trend seems to explain the formation of binary compounds MSb_3 with increasing thermal stability in the sequence from Co, Rh to Ir. Thus only $Yb_xFe_4Sb_{12}$ may be considered as a true ternary compound, whereas the remaining compounds eventually represent an extension of a stable binary phase into the ternary system.

3.2 Transport properties

Figure 2a displays the temperature dependent resistivity, normalised to room temperature for compounds with M = Co and Fe. This group of materials exhibits metallic behaviour with smoothly increasing resistivity values on increasing temperature. However, $Yb_{0.2}Co_4Sb_{12}$ is

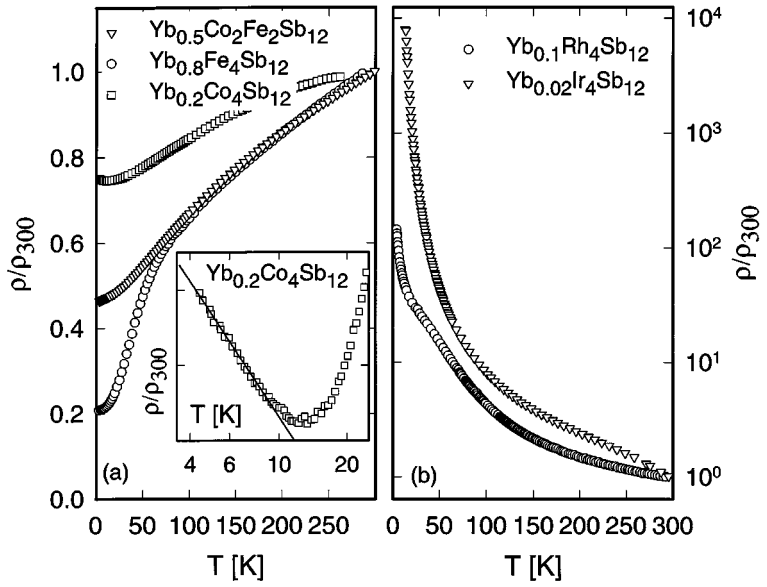

Fig. 2. Normalised temperature dependent resistivity ρ/ρ_{300} of $Yb_xM_4Sb_{12}$. The inset of Figure 2a shows in detail the low temperature behaviour of $Yb_{0.2}Co_4Sb_{12}$ on a logarithmic temperature scale.

characterised by a shallow minimum in $\rho(T)$ around $T =$ 10 K and the resistivity starts to increase below that temperature. Roughly, a logarithmic behaviour is deduced, reminiscent of Kondo type interactions at low temperatures (inset, Fig. 2a). In agreement with a previous study by Dilley *et al.* [8], $\rho(T)$ of $Yb_{0.8}Fe_4Sb_{12}$, displays a broad shoulder at about 60 to 80 K and below this temperature there is a substantial resistivity drop, indicative of, presumably, electron scattering on a narrow feature in the electronic density of states in the proximity to the Fermi energy.

The absolute resistivity is found to increase from $Yb_{0.8}Fe_4Sb_{12}$ ($\rho_{RT} \approx 460$ $\mu\Omega$ cm) to $Yb_{0.5}Co_2Fe_2Sb_{12}$ ($\rho_{RT} \approx 1850$ $\mu\Omega$ cm). As will be discussed in detail in the next paragraph, the Co/Fe substitution and the decrease of Yb in this sequence reduces the number of holes, hence conductivity decreases. No regular shaped samples could be prepared in the case of $Yb_{0.2}Co_4Sb_{12}$, therefore no absolute resistivity values were obtained.

Both, from bandstructure calculations [19] and from the experimental point of view [20] a semiconducting behaviour was deduced for $CoSb_3$ ($\Delta E \approx 50$ meV, ΔE: energy gap at $E = E_F$). A reasonable number of Yb ions in the voids of the skutterudite structure thus provides for $Yb_xCo_4Sb_{12}$ enough free carriers to shift the material into a metallic state as deduced from our resistivity measurement. If Co is replaced by Fe, holes in the valence band are created. Additionally, the Yb content increases as the Fe content grows. Thus the supplied electrons, however, compensate just partially some of these holes and the conductivity should remain p-type. If, in a first approximation, Yb is assumed to be trivalent, $Yb_{0.8}Fe_4Sb_{12}$ should have, in terms of simple crystal chemistry, a hole concentration of about 1.6 holes per formula unit, while such a hole count reveals about 0.5 for $Yb_{0.5}Co_2Fe_2Sb_{12}$. The smaller number of holes in the latter, of course, yields larger overall resistivity values, in agreement with the experiment. A similar scenario has already been discussed in detail in the case of $Ce_xFe_{4-y}Co_ySb_{12}$ [13], and a crossover from a semiconducting to metallic behaviour was deduced on an increase of the Fe content, which concomitantly yields an increase of Ce in the cages. However, different to the Ce based series, $Yb_xFe_{4-y}Co_ySb_{12}$ stays metallic throughout the concentration range studied. In the simplest picture, this could be related to the intermediate valence of the Yb ion, where the reduced number of free electrons is unable to fully compensate the holes created by the Co/Fe substitution, thus metallic (p-type) behaviour is possible in the whole substitution range.

The temperature dependent resistivity of $Yb_xRh_4Sb_{12}$, $x \approx 0.1$ and $Yb_xIr_4Sb_{12}$, $x \approx 0.02$ is shown in Figure 2b, again in a normalised representation. Different to the group with M = Fe, Co, these compounds exhibit a semiconducting behaviour where the resistivity increases over some orders of magnitude from room temperature to 4 K. Applying an activation-type model to describe $\rho(T)$ in this case, *i.e.*, $\rho = \rho_0 \exp(\Delta E/2k_BT)$, allows us to estimate the gap width ΔE of the electronic density of states (DOS) at the Fermi energy E_F. A least squares fit to the data above about 100 K reveals $\Delta E = 368$ K for M = Rh and $\Delta E = 277$ K for M = Ir. A comparison of all resistivity measurements infers a close relation of the ground state behaviour with the Yb content determined from Rietveld refinement in the various samples: while for $x \geq 0.2$ metallic behaviour is observed, the smaller Yb content in the skutterudite phase for the Rh and the Ir compound preserves a semiconducting state, with a band gap of roughly 33 and 25 meV for the Rh and the Ir compound, respectively. Previously performed low temperature resistivity measurements [21] on the unfilled binary $IrSb_3$ revealed also a semiconducting type of behaviour, corresponding to a narrow band gap of about 10 meV,

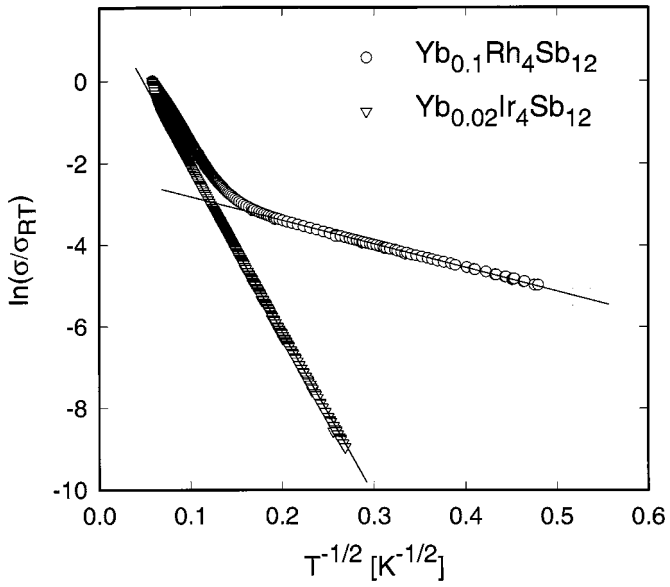

Fig. 3. $\ln(\sigma/\sigma_{300\mathrm{K}})$ *versus* $T^{-1/2}$ of $Yb_{0.1}Rh_4Sb_{12}$ and $Yb_{0.02}Ir_4Sb_{12}$. Solid lines are least squares fits of the data in the low temperature region according to equation (2).

in agreement to band structure calculations of Sing and Pickett [22] predicting $IrSb_3$ as essentially a zero gap semiconductor. Roughly above 100 K, $IrSb_3$ was reported to behave metallic like.

However, as it is obvious from Figure 2b, a shoulder type structure occurring roughly around 50 K marks the end of the validity of an activation type behaviour. In order to account also for the temperature range below, we have tried to invoke Mott's model of variable range hopping [23], *i.e.*,

$$\sigma = \sigma_0 \exp\left[-\left(\frac{T_{1/4}}{T}\right)^{1/4}\right], \qquad (1)$$

where $\sigma \equiv 1/\rho$, σ_0 is a material constant and $T_{1/4}$ is the characteristic temperature of the system. Least squares fits of equation (1) to the data yield reasonable agreement only in a narrow temperature interval. An expression of the form

$$\sigma = \sigma_0 \exp\left[-\left(\frac{T_{1/2}}{T}\right)^{1/2}\right], \qquad (2)$$

on the contrary, seems to describe the conductivity data over a substantial larger temperature range as it is obvious from a plot of $\ln(\sigma/\sigma_{\mathrm{RT}})$ *vs.* $T^{-1/2}$ for both $Yb_{0.1}Rh_4Sb_{12}$ and $Yb_{0.02}Ir_4Sb_{12}$ (see Fig. 3). The characteristic temperature $T_{1/2}$ is 38 and 1700 K, respectively. The main difference between equations (1) and (2) is the exponent, where the latter is appropriate for a variable range hopping in the presence of a Coulomb gap [24,25], *i.e.*, when the single-particle density of states close to the chemical potential is depleted due to the Coulomb interaction between electrons.

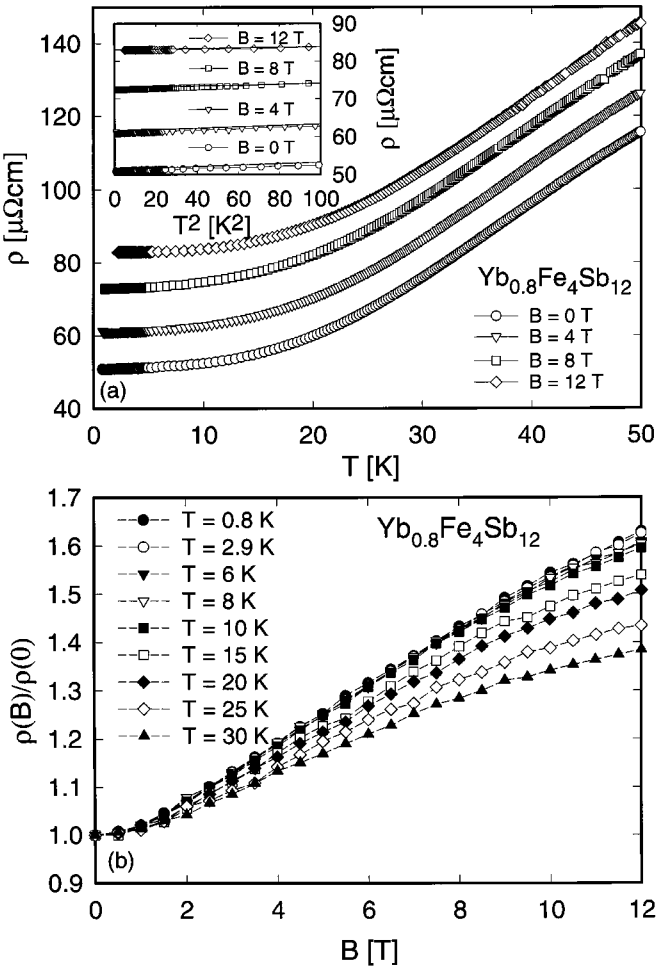

Fig. 4. (a) Temperature dependent resistivity ρ of $Yb_{0.8}Fe_4Sb_{12}$ for various applied fields. The inset shows $\rho(T)$ as a function of T^2. (b) Field dependent magnetoresistance of $Yb_{0.8}Fe_4Sb_{12}$ for various temperatures.

In order to study the field response of Yb based skutterudites, we have performed resistivity measurements in a temperature range from about 1 K to 100 K and fields up to 12 T. Results are shown for $Yb_{0.8}Fe_4Sb_{12}$ in Figures 4a and 4b. The most prominent feature of these measurements is a positive magnetoresistance in the whole temperature and field range covered. Moreover, the positive magnetoresistance is large, even at high temperature. As already indicated in reference [8], the resistivity of $Yb_{0.8}Fe_4Sb_{12}$ is reminiscent of strongly correlated electron systems, where scattering into a large narrow feature in the electronic density of states, with presumably f-character, occurs. Usually, such a scattering may be accounted for in terms of the phenomenological Fermi liquid model; accordingly the low temperature resistivity should behave proportional to T^2, *i.e.*, $\rho = \rho_0 + AT^2$. In the inset of Figure 4a we plotted the resistivity on a quadratic temperature scale. Indeed, $\rho(T)$ varies proportional to T^2. The range of validity, however, increases with increasing fields while the coefficient A substantially decreases. Figure 4b shows $\rho(B)/\rho(0)$ *vs.* B, where $\rho(B)$ and $\rho(0)$ are

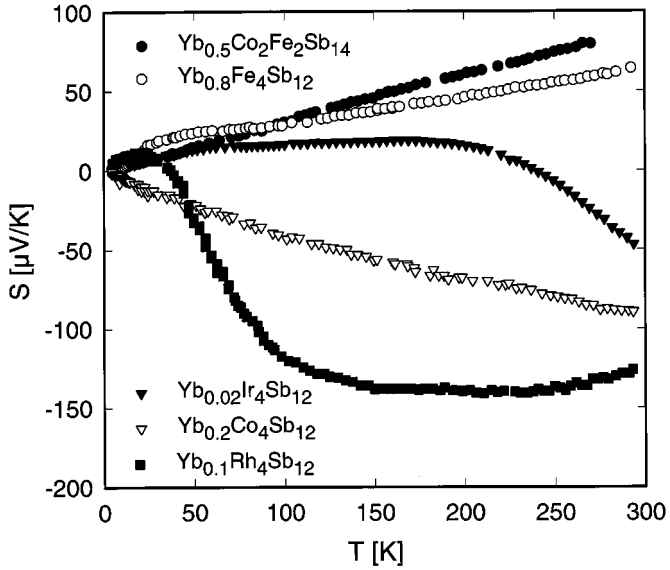

Fig. 5. Temperature dependent thermopower S of$Yb_xM_4Sb_{12}$.

respectively the resistivities with and without field. This type of measurement clearly indicates the increase of $\rho(T)$ in the covered temperature range upon an increasing magnetic field. Usually, such a positive magnetoresistance can be associated with the classical cyclotron motion of carriers forced by the applied magnetic field.

In Figure 5, the thermoelectric power $S(T)$ is displayed for all the compounds investigated. Throughout this series, positive and negative thermopower is observed, reaching values of about $+90$ μV (at room temperature) in the case of $Yb_{0.5}Co_2Fe_2Sb_{14}$, and about -150 μV (at about 200 K) in the case of $Yb_{0.1}Rh_4Sb_{14}$. While $S(T)$ of $Yb_{0.5}Co_2Fe_2Sb_{14}$ and $Yb_{0.2}Co_4Sb_{14}$ varies almost linearly, there is a non-linear temperature dependence in the remaining compounds. It is interesting to note that $Yb_{0.5}Co_2Fe_2Sb_{12}$ exhibits larger thermopower values than $Yb_{0.8}Fe_4Sb_{12}$. This is most likely related to the fact that the number of holes is reduced from 4 to 2 by the Co/Fe substitution (in terms of crystal chemistry) and moreover, electrons provided by Yb further reduce the hole number to about 0.5, if Yb is assumed to be trivalent. In the case of intermediate valence of the Yb ion, the final hole count in this particular compound can be slightly larger. A similar procedure performed for $Yb_{0.8}Fe_4Sb_{12}$ yields $n \geq 1.6$. In any case, the smaller number of carriers gives rise to larger thermopower values. Eventually, if $Yb_{0.2}Co_4Sb_{12}$ is attained, the sign of the thermopower becomes negative, indicating the crossover from a p-type metal to n-type behaviour. Comparable n-type compounds in this group of materials like $La_{0.05}Co_4Sb_{12}$ or $La_{0.23}Co_4Sb_{12}$ [15] exhibit almost the same temperature dependent thermopower, supporting in a first approximation the mentioned crossover from p to n-type conductivity in the present Yb series. The binary starting material $CoSb_3$ shows only positive $S(T)$ values, reaching about 190 μV/K at room temperature [15]. Furthermore, it seems to be of interest to note that the absolute thermopower of M = Rh exceeds that of M = Co for higher temperatures ($T > 50$ K). Again this may be taken as evidence for a higher carrier density in M = Co based on the higher Yb content. Absolute values observed throughout this series are only moderately enhanced; technical applicability would require increasing these values up to $S \geq 160$ μV. The latter would be sufficient, if the Wiedemann Franz law is valid, to infer values of the figure of merit $ZT \approx 1$.

Measurements of the thermal conductivity for some of the $Yb_xM_4Sb_{12}$ compounds are summarised in Figure 6a. In general, the observed thermal conductivity is small and the upper limit at room temperature does not exceed 60 mW/cmK, which has to be compared with the theoretical minimum thermal conductivity evaluated for skutterudite type material of about 7 mW/cmK [9]. $Yb_xIr_4Sb_{12}$ with $x \approx 0.02$ shows a room temperature thermal conductivity below 20 mW/cmK. The upturn of $\lambda(T)$ observed experimentally for $T > 200$ K is supposed to follow primarily from radiation losses of the sample due to incomplete shielding in the measuring device. Therefore, the following treatment of the conductivity data is restricted to the temperature region below 150 K where the temperature gradient between sample and shielding is negligible.

The total thermal conductivity λ is usually given by $\lambda = \lambda_e + \lambda_l$ where λ_e represents the electron (hole) part and λ_l the lattice contribution. In the case of simple metals, the Wiedemann Franz law is expected to be valid, thus, $\lambda_e = L_0 T/\rho$. $L_0 = 2.45 \times 10^{-8}$ W/ΩK^{-2} is the Lorenz number (derived in the scope of the free electron model) and ρ is the electrical resistivity of the sample. The specific Lorenz number of a doped semiconductor, however, depends upon the Fermi energy and the band gap [26]. In the case of La- and Ce containing skutterudite materials a slightly modified Lorenz number $L_0 = 2 \times 10^{-8}$ W/ΩK^{-2} has hitherto been accepted as an appropriate value [9].

Applying the Wiedemann Franz law to systems other than simple metals in order to separate λ_e and λ_l results in only crude approximations; nevertheless it is widely used in the field of thermoelectric materials (compare Ref. [9]). λ_l follows then simply from $\lambda_l = \lambda - L_0 T/\rho$. Results of such an analysis are shown in Figure 6b for two extreme cases between metallic ($Yb_{0.8}Fe_4Sb_{12}$) and semiconducting behaviour ($Yb_{0.1}Rh_4Sb_{12}$). In Figure 6b, the larger symbols refer to the total measured conductivity of $Yb_{0.8}Fe_4Sb_{12}$ and $Yb_{0.1}Rh_4Sb_{12}$, while the smaller filled and open symbols refer to the lattice and the electronic thermal conductivity, respectively. Accordingly, λ_e is almost negligible in the case of semiconducting $Yb_{0.1}Rh_4Sb_{12}$, while there is a substantial contribution to the total measured effect for metallic $Yb_{0.8}Fe_4Sb_{12}$.

3.3 Magnetic properties

Shown in Figure 7 is the inverse magnetic susceptibility $\chi^{-1}(T)$ of $Yb_xM_4Sb_{12}$ as a function of temperature. Above about 50 K $\chi(T)$ can be reasonably well described by a modified Curie-Weiss law $\chi(T) = \chi_0 + C/(T - \theta_p)$

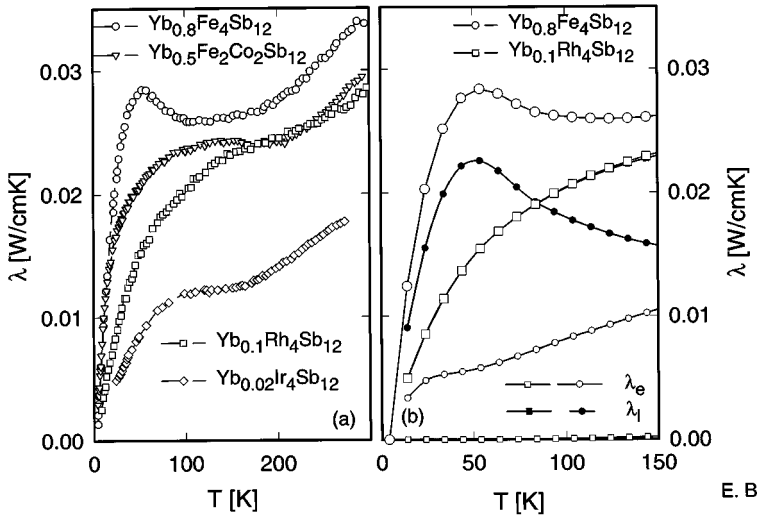

Fig. 6. (a) Temperature dependent thermal conductivity λ of Yb$_x$M$_4$Sb$_{12}$. (b) Separation of the total thermal conductivity into the electronic and lattice contributions for M = Fe and M = Rh.

Table 2. Effective magnetic moment $\mu_{\rm eff}$, paramagnetic Curie temperature $\theta_{\rm p}$, magnetisation M at $T = 2$ K and $\mu_0 H = 6$ T.

	$\mu_{\rm eff}$ [$\mu_{\rm B}$/f.u]	$\theta_{\rm p}$ [K]	$M(H = 6$ T) [$\mu_{\rm B}$/f.u]	Ref.
$YbFe_4Sb_{12}$	3.09	40	0.52	[8]
$Yb_1Fe_4Sb_{12}$	4.49	13.8	1.43	[11]
$Yb_{0.8}Fe_4Sb_{12}$	3.36	26.5	0.82	this work
$Yb_{0.5}Fe_2Co_2Sb_{12}$	2.75	−10	1.04	this work
$Yb_{0.2}Co_4Sb_{12}$	2.6	−9	0.93	this work
$Yb_{0.1}Rh_4Sb_{12}$	3.40	−36	0.76	this work
$Yb_{\approx 0}Ir_4Sb_2$	3.10	−25	0.87	this work

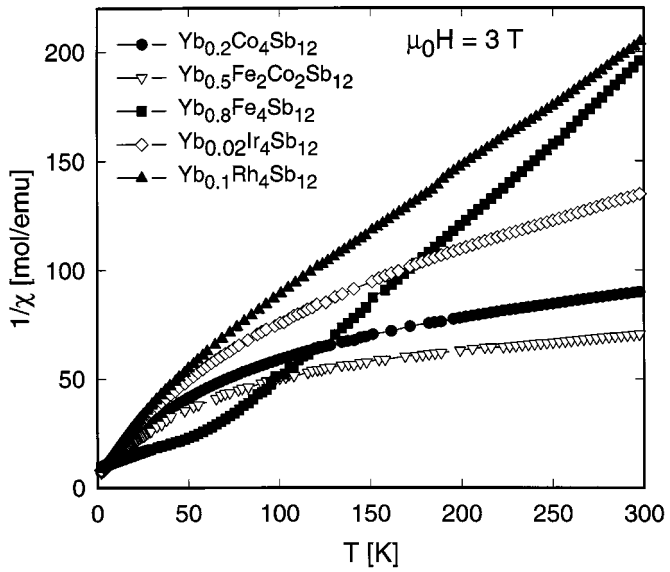

Fig. 7. Temperature dependent inverse magnetic susceptibility χ^{-1} of Yb$_x$M$_4$Sb$_{12}$ at $\mu_0 H = 3$ T.

with C the Curie constant, $\theta_{\rm p}$ the paramagnetic Curie temperature and a temperature independent susceptibility contribution χ_0. The results of least squares fits are summarised in Table 2. The comparison of the Yb deficient compound $Yb_{0.8}Fe_4Sb_{12}$ with the available literature data of $YbFe_4Sb_{12}$ [8,11] indicates that the Yb content may be of importance for the variation of $\mu_{\rm eff}$, $\theta_{\rm p}$, and $M_{\rm sat}$ (although the lattice parameters hardly differ). The effective magnetic moment, $\mu_{\rm eff}$, of Yb$_x$M$_4$Sb$_{12}$ is significantly below that of the free Yb^{3+} ion ($\mu_{\rm eff}$ = 4.54 $\mu_{\rm B}$) which implies that Yb exhibits an intermediate valence due to an electronic configuration between the $4f^{14}$ and the $4f^{13}$ state. In fact, recently performed $L_{\rm III}$ measurements on $YbFe_4Sb_{12}$ revealed a mixture of the Yb 2+ and 3+ state, thus giving a valence $\nu \approx 2.68$ [11]. On the other hand the low temperature magnetic isotherms of $Yb_{0.8}Fe_4Sb_{12}$, displayed in Figure 8, show a significant initial curvature indicative of the presence of local moments, presumably due to magnetic impurities of the order of 0.26 $\mu_{\rm B}$/f.u.. Such a behaviour was also observed for $YbFe_4Sb_{12}$ [8] with a moment of 0.2$\mu_{\rm B}$ assigned to magnetic impurities. This feature is not as pronounced

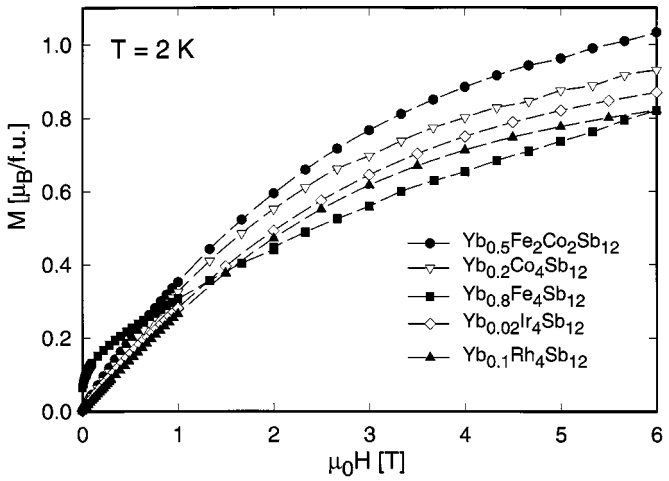

Fig. 8. Isothermal magnetization of $Yb_xM_4Sb_{12}$ at $T = 2$ K.

for the other compounds investigated where an approximate scaling of the magnetic isothermes with H/T is observed for $T > 15$ K. The deviation from the H/T scaling of the $M(H)$ curves for temperatures below 15 K is indicative of magnetic correlations presumably due to magnetic impurities. Furthermore, only $Yb_{0.8}Fe_4Sb_{12}$ exhibits a positive paramagnetic Curie temperature while the θ_p values are negative for the other compounds, consistent with the strongly positive paramagnetic Curie temperature derived from $La_{0.9}Fe_3CoSb_{12}$ [9]. This crossover from ferro- to antiferromagnetic interactions may be simply due to the influence of the impurity phases still contributing to the bulk magnetic properties.

Unfortunately, the parent Fe_4Sb_{12} compound cannot be synthesised, but from the bulk effective moments of $LaFe_4Sb_{12}$ ($\mu_{eff} = 3$ μ_B/f.u.) [5] and $La_{0.9}Fe_3CoSb_{12}$ $\mu_{eff} = 2.52$ μ_B/f.u.) [9] it is obvious that the $[Fe_{4-x}Co_xSb_{12}]$ polyanion carries a finite effective magnetic moment depending on the electron concentration. This was also demonstrated by susceptibility and transport measurements of $Ce_x(Fe, Co)_4Sb_{12}$ by Sales *et al.* [9] where the electron concentration depends not only on the Fe/Co ratio but also upon the valence and the content of Ce. Danebrock *et al.* [5] proposed from a comparative susceptibility study on various $REFe_4Sb_{12}$ and $EPFe_4Sb_{12}$ compounds (RE: rare earth, EP: electropositive elements) that the paramagnetic moment of the Fe_4Sb_{12} polyanion depends on the charge transfer from RE or EP $\rightarrow$ $[Fe_4Sb_{12}]$ which compensates partially the four low-spin d^5 states of Fe^{3+} in a hypothetical Fe_4Sb_{12} compound. This model was questioned by Leithe-Jasper *et al.* [11] since Mössbauer experiments revealed a Fe^{2+} low spin d^6 configuration for $YbFe_4Sb_{12}$. A comparison of the collected available data for $Yb_xFe_4Sb_{12}$ in Table 2 indicates the scatter of the bulk effective- and low temperature moments which can be attributed to an appreciable amount of unresolved magnetic impurities if the given Yb content is correct.

In contrast to $Yb_xFe_4Sb_{12}$ where the variation of μ_{eff} depends sensitively on the Yb content, it is noteworthy that the other compounds investigated exhibit similar effective magnetic moments ranging between 2.6 and 3.1 μ_B/f.u. and appear to be almost independent of the particular Yb content in the skutterudite phases. It is therefore of interest to check the contribution of the unfilled skutterudites Co_4Sb_{12}, Ir_4Sb_{12} and Rh_4Sb_{12}. According to Gajewski *et al.* [7] Co_4Sb_{12} is diamagnetic with $\chi \approx -4 \times 10^{-4}$ cm^3/(mol f.u.) and $Fe_{0.2}Co_{3.8}Sb_{12}$ contains some local moment magnetism but χ_0 saturates to a value of about 3.2×10^{-3} cm^3/(mol f.u.) at low temperatures. Ir_4Sb_{12} and Rh_4Sb_{12} are characterised by a diamagnetic susceptibility of -5.8×10^{-4} emu/mol and -4.9×10^{-4} emu/mol, respectively, where the low temperature upturn of $\chi(T)$ can be attributed to an effective moment of about 0.35 μ_B/f.u. due to impurities. Accordingly, the magnetic isotherms exhibit a significant curvature, particularly at low temperatures (inset, Fig. 8 for Rh_4Sb_{12}), but are still dominated by the diamagnetic contribution yielding the negative slope at higher fields. Similar observations were made for $IrSb_3$. Diamagnetic behaviour was reported also in the case of a filled Ir based skutterudite, *i.e.*, $LaIr_4Ge_3Sb_9$ [12]. In the latter example, the substitution of La by Nd causes an effective magnetic moment which corresponds exactly to the moment of the trivalent Nd ion [12]. The crossover from dia- to paramagnetic behaviour for the corresponding filled skutterudites $Yb_xM_4Sb_{12}$ (M = Co, Rh, Ir) cannot unambiguously be attributed to electronic changes of the polyanionic framework M_4Sb_{12} since secondary phases (*e.g.* Yb_2O_3) and/or magnetic impurities in the grain boundaries may still contribute to the bulk magnetic properties measured. Although such magnetic impurities could be neither detected by EMPA nor with X-ray analyses, they seem to be present because otherwise significantly different Yb concentrations should cause magnetic changes of similar magnitude in the M_4Sb_{12} sublattice or if the latter is assumed to remain diamagnetic, unreasonably high effective moments/Yb would be the consequence.

3.4 Specific heat

Specific heat measurements on selected bulk samples of the filled skutterudites, *i.e.* $Yb_{0.8}Fe_4Sb_{12}$, $Yb_{0.5}Fe_2Co_2Sb_{12}$ and $Yb_{0.1}Rh_4Sb_{12}$, as well as on the binary skutterudites, *i.e.* $RhSb_3$ and $IrSb_3$, were performed from 2 to 60 K in order to study the effect of Yb doping upon the electronic – and in particular the lattice contributions. Besides the electronic and vibrational changes, a magnetic contribution is obvious for $Yb_xM_4Sb_{12}$, which presumably arises from Yb^{3+} ions as manifested by the pronounced low temperature upturn of the specific heat, $C(T)/T$ *vs.* T^2, depicted in Figure 9, where we use the formula M_4Sb_{12} also for the binary skutterudites in order to simplify the comparison of the molar heat capacities. The fact that the magnetic contribution of $YbFe_4Sb_{12}$ reported by Dilley *et al.* [8] is significantly smaller than for the present $Yb_{0.8}Fe_4Sb_{12}$ sample, prepared with the same nominal composition $Yb_1Fe_4Sb_{12}$, most likely indicates that the Yb loss of 0.2Yb/f.u. is partly bound

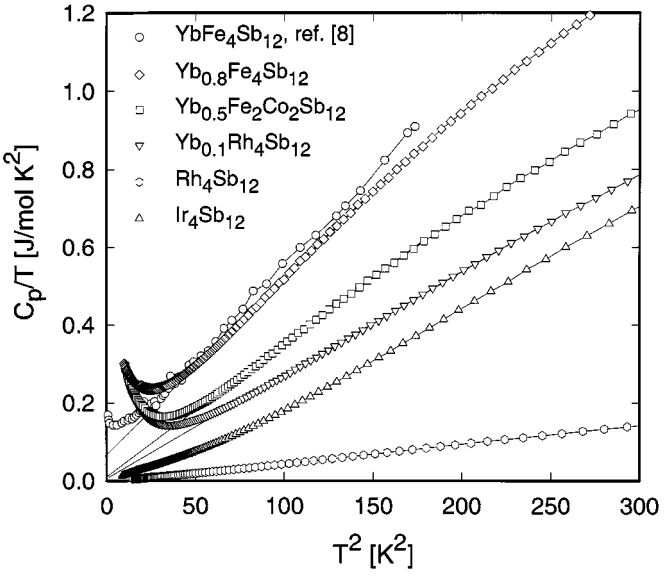

Fig. 9. Low temperature heat capacity, $C(T)/T$ *vs.* T^2, of Yb$_x$M$_4$Sb$_{12}$ and M$_4$Sb$_{12}$. YbFe$_4$Sb$_{12}$ data given in reference [8] are shown for comparison. The solid lines show a tentative extrapolation of the electronic and lattice contribution towards zero temperature.

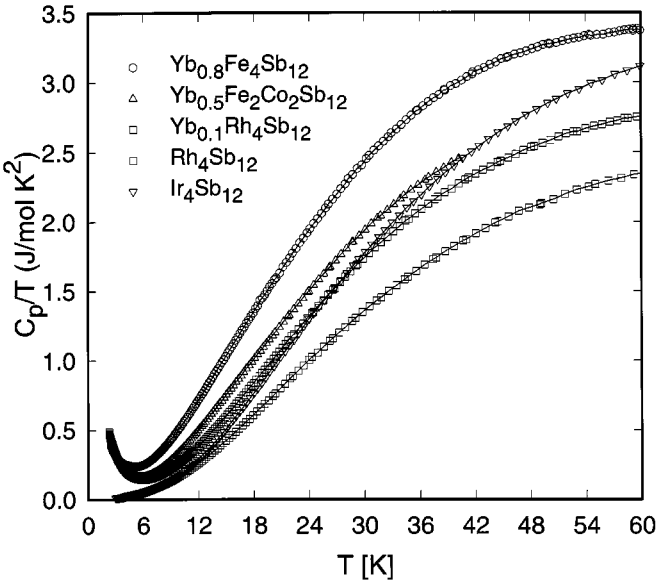

Fig. 10. The specific heat, $C(T)/T$ *vs.* T, of Yb$_x$M$_4$Sb$_{12}$ and M$_4$Sb$_{12}$ up to 60 K.

in form of magnetic secondary phases. The low temperature specific heat data further reveal that the extrapolated γ-value (see the solid lines in Fig. 9) is close to zero ($\gamma < 10$ mJ/mol K^2) except for Yb$_{0.8}$Fe$_4$Sb$_{12}$ where a conduction electron contribution corresponding to $\gamma \sim 60$ mJ/mol K^2 is indicated.

As already noted in the introduction, the primary intention of Yb-doping is to change the vibrational properties by introducing local "rattling" modes and thereby to reduce the thermal conductivity. Thus, we present in Figure 10 the specific heat, $C(T)/T$ *vs.* T, up to 60 K which shows – above 6 K – nearly exclusively the lattice heat capacity. Note, even for Yb$_{0.8}$Fe$_4$Sb$_{12}$ the electronic contribution is just of the order of the size of the symbols used in Figure 10. The analysis of the specific heat of the binary skutterudites RhSb$_3$ and IrSb$_3$ reveals that a combination of one Debye- and two Einstein functions which can be adjusted *via* the equation

$$C_{\rm ph}(T) = 4\frac{9R}{\omega_{\rm D}^3}\int_0^{\omega_{\rm D}} \frac{\omega^2\left(\frac{\omega}{2T}\right)^2}{\sinh^2\left(\frac{\omega}{2T}\right)}{\rm d}\omega + \sum_{i=1,2} c_i R \frac{\left(\frac{\omega_{E_i}}{2T}\right)^2}{\sinh^2\left(\frac{\omega_{E_i}}{2T}\right)} \quad (3)$$

with $c_1 = 27$ and $c_2 = 9$ yields already a reasonable parameterisation of the whole temperature dependence from 2–60 K. Thereby, the three acoustic and nine optical branches of the phonon dispersion of MSb$_3$ are represented by (12×) one Debye- and two Einstein functions ($27 \times f_{E_1} + 9 \times f_{E_2}$) corresponding to the formula M$_4$Sb$_{12}$ used in Figure 10. Thus, for a straight forward comparison of the binary and ternary skutterudites we simply have to add one further Einstein function for the latter accounting for the increased number of phonon modes due to the additional x atoms per f.u. of Yb$_x$M$_4$Sb$_{12}$, *i.e.* the index to the sum in relation (3) is $i = 1, 2, 3$ with $c_3 = 3x$. The parameters obtained by least squares fits of the experimental data are summarised in Table 3 together with the Debye temperature values, $\Theta_{\rm D} = \sqrt[3]{1944(16+x)/\beta}$, where β is the slope of C/T *vs.* T^2 as indicated by the solid lines in Figure 9. The comparison of these results reveals a very pronounced softening of major parts of the phonon spectrum (see $\omega_{\rm D}$ and ω_{E_1} which carry the major part of spectral weight). Comparing RhSb$_3$ and Yb$_{0.1}$Rh$_4$Sb$_{12}$ we see that already a small filling level causes a dramatic softening of the lattice which can not simply be attributed to a "rattling" mode by the Yb atoms because the corresponding spectral weight would be clearly too small to account for the large change of the lattice's heat capacity. The same argument also excludes that these large changes be due to the small amount of secondary phases which originate from some excess of ytterbium. The overall effect of the lattice softening is further strengthened by the trend seen for Yb$_{0.5}$Fe$_2$Co$_2$Sb$_{12}$ and Yb$_{0.8}$Fe$_4$Sb$_{12}$ where despite the lighter metal atoms (3*d*-M instead of the Rh 4*d*-metal) still a further reduction of the mean phonon energy is observed. Note, for the two binary examples RhSb$_3$ and IrSb$_3$ the mass effect is even larger than expected by the simple relation $\Theta_{\rm D} \propto 1/\sqrt{m}$ where m is the mean atomic mass.

3.5 Figure of merit

Beside the basic electronic and magnetic properties, described above, skutterudite-type materials are considered as candidates for thermoelectric applications. In such a case, the figure of merit ZT should be as large as possible

Table 3. Results of the Debye/Einstein analysis of the lattice heat capacities as explained in the text. (*) marks contributions which are hardly significant because of the small spectral weight.

	Θ_D (K)	ω_D (K)	ω_{E_1} (K)	ω_{E_2} (K)	ω_{E_3} (K)
$IrSb_3$	269	152	235	163	–
$RhSb_3$	407	162	334	167	–
$Yb_{0.1}Rh_4Sb_{12}$	~ 230	142	280	160	150*
$Yb_{0.5}Fe_2Co_2Sb_{12}$	~ 210	130	264	173	150*
$Yb_{0.8}Fe_4Sb_{12}$	~ 190	123	262	143	143

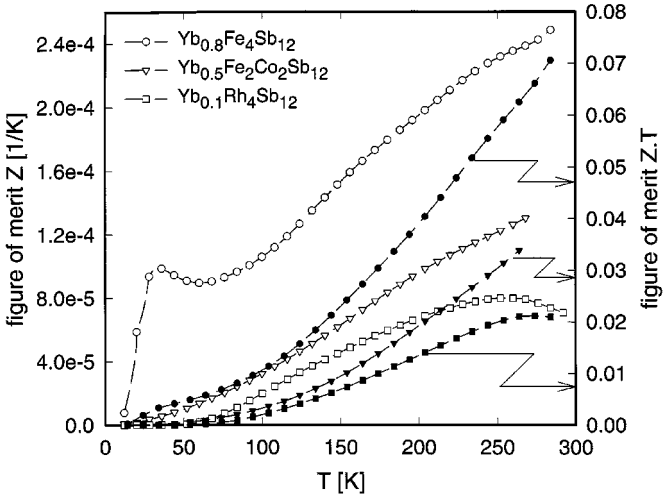

Fig. 11. Temperature dependent figure of merit Z and ZT for $Yb_xM_4Sb_{12}$n M = Fe, FeCo, Rh.

and various groups of semiconducting materials exhibit above room temperature $ZT \approx 1$. $Ce_{0.9}Fe_3CoSb_{12}$ as one of the best studied examples in the group of rare earth filled skutterudites shows a strong temperature dependent behaviour of ZT. At room temperature, $ZT \approx 0.2$, while roughly around 700 °C, ZT approaches a value of 1 [9]. In Figure 11 the figure of merit for some of the investigated Yb-filled skutterudites is shown. The open symbols refer to Z *vs.* T (left axis), while the filled symbols represent ZT *vs.* T. The largest value of ZT at room temperature is found for $Yb_{0.8}Fe_4Sb_{12}$, and it is expected that ZT grows further with growing temperature. However, the actual value is roughly 5 times smaller when compared to $Ce_{0.9}Fe_3CoSb_{12}$. This reduced magnitude of ZT can possibly be attributed to the large resistivity values observed for the particular sample measured, about 450 $\mu\Omega$ cm at room temperature, which is roughly 5 times larger than the resistivity of $YbFe_4Sb_{12}$ reported by Dilley *et al.* [8] for their sample. Such a factor would mean that ZT of $Yb_{0.8}Fe_4Sb_{12}$ can be of comparable magnitude to $Ce_{0.9}Fe_3CoSb_{12}$. It is thought that the larger resistivity of the present sample is due to the lower density of our sintered material with respect to the melted material of Dilley *et al.* [8]. In our evaluation of the figure of merit it is noteworthy to mention that incomplete shielding above 200 K resulted in overestimated thermal conductivity values which consequently reveals somewhat reduced values Z at $T > 200$ K.

4 Summary

The isotypic compounds $Yb_xM_4Sb_{12}$, M = Fe, Co, FeCo, Rh, Ir, revealed physical properties (*e.g.*, electrical resistivity, thermopower) which seem to systematically correlate with a) the degree of filling of the icosahedral voids in the skutterudite lattice by Yb and b) the electronic change as a function of the Fe/Co substitution, *i.e.*, the number of uncompensated hole carriers. The ground state behaviour is found to simply depend on the particular number of Yb atoms in the unit cell, reflected by a crossover from a semiconducting to a metallic state for $x > 0.1$. Thermoelectric power at room temperature in this series ranges from +90 μV to about −150 μV, which for unoptimized systems exhibits already attractive features for possible technological applications in thermopower conversion devices.

Part of this research was sponsored by the Austrian FWF under grant number P13778 as part of a HCM-network and P12899.

References

1. M.S. Torikachivili, J.W. Chen, Y. Dalichaouch, R.P. Guertin, M.W. McElfresh, C. Rossel, M.B. Maple, G.P. Meisner, Phys. Rev. B **36**, 8660 (1987).
2. I. Shirotani, T. Adachi, K. Tachi, S. Todo, K. Nozawa, T. Yagi, and M. Kinoshita, J. Phys. Chem. Solids **57**, 211 (1996).
3. I. Shirotani, T. Uchiumi, K. Ohno, C. Sekine, Y. Nakazawa, K, Kanoda, S. Todo, T. Yagi, Phys. Rev. B **56**, 7866 (1997).
4. C. Sekine, T. Uchiumi, I. Shirotani, T. Yagi, Phys. Rev. Lett. **79**, 3218 (1997).
5. M.E. Danebrock, C.B.H. Evers, W. Jeitschko, J. Phys. Chem. Solids **57**, 381 (1996).
6. D.T. Morelli, G.P. Meisner, J. Appl. Phys. **77**, 3777 (1995).

7. D.A. Gajewski, M.R. Dilley, E.D. Bauer, E.J. Freeman, R. Chau, M.B. Maple, D. Mandrus, B.C. Sales, A.H. Lacerda, J. Phys. Cond. Matter **10**, 6973 (1998).
8. N.R. Dilley, E.J. Freeman, E.D. Bauer, M.B. Maple, Phys. Rev. B **58**, 6287 (1998).
9. B.C. Sales, D. Mandrus, B.C. Chakoumakos, V. Keppens, J.R. Thompson, Phys. Rev. B **56**, 15081 (1997).
10. G.A. Slack, *CRC Handbook of Thermoelectrics*, edited by D.M. Rowe (Chemical Rubber, Boca Raton, Fl. 1995), Chap. 34, p. 407.
11. A. Leithe-Jasper, D. Kaczorowski, P. Rogl, J. Bogner, M. Reissner, W. Steiner, G. Wiesinger, C. Godart, Solid State Commun. **109**, 395 (1999).
12. G.S. Nolas, G.A. Slack, D.T. Morelli, T.M. Tritt, A.C. Ehrlich, J. Appl. Phys. **79**, 4002 (1996).
13. B. Chen, J.H. Xu, C. Uher, D.T. Morelli, G.P. Meissner, J.P. Fleurial, T. Caillat, A. Borshchevsky, Phys. Rev. B **55**, 1476 (1997).
14. D.T. Morelli, G.P. Meisner, B. Chen, S. Hu, C. Uher, Phys. Rev. B **56**, 7376 (1997).
15. G.S. Nolas, J.L. Cohn, G.A. Slack, Phys. Rev. B **58**, 164 (1998).
16. W. Wacha, program STRUKTUR, Diploma thesis TU-Vienna, 1989.
17. J. Rodriguez-Carvajal, *FULLPROF: A Program for Rietveld Refinement and Pattern Matching Analysis, Abstracts of the Satellite Meeting on Powder Diffraction of the XV Congr. Intl. Union of Crystallogr., Talence, France*, p. 127.
18. W. Jeitschko, D.J. Braun, Acta Crystallogr. B **33**, 3401 (1977).
19. J.L. Feldmann, J.D. Singh, Phys. Rev. B **53**, 6273 (1996).
20. D. Mandrus, A. Migliori, T.W. Darling, M.F. Hundley, E.J. Peterson, J.D. Thompson, Phys. Rev. B **52**, 4926 (1995).
21. T.M. Tritt, G.S. Nolas, G.A. Slack, A.C. Ehrlich, D.J. Gillespie, J.L. Cohn, J. Appl. Phys. **79**, 8412 (1996).
22. D.J. Singh, W.E. Picket, Phys. Rev. B **50**, 11235 (1995).
23. N.F. Mott, J. Non-Cryst. Solids **1**, 1 (1968).
24. A.L. Efros, B.I. Shklovskii, J. Phys. C **8**, L49 (1975).
25. A.L. Efros, J. Phys. C **9**, 202 (1976).
26. C.M. Bhandari, *CRC Handbook of Thermoelectrics*, edited by D.M. Rowe (Chemical Rubber, Boca Raton, Fl. 1995), Chap. 6, p. 55.